

# We are IntechOpen, the world's leading publisher of Open Access books Built by scientists, for scientists

6,900

Open access books available

186,000

International authors and editors

200M

Downloads

Our authors are among the

154

Countries delivered to

TOP 1%

most cited scientists

12.2%

Contributors from top 500 universities



WEB OF SCIENCE™

Selection of our books indexed in the Book Citation Index  
in Web of Science™ Core Collection (BKCI)

Interested in publishing with us?  
Contact [book.department@intechopen.com](mailto:book.department@intechopen.com)

Numbers displayed above are based on latest data collected.  
For more information visit [www.intechopen.com](http://www.intechopen.com)



---

# Carbon Nanotubes Filled With Ternary Chalcogenides

---

Marian Nowak and Marcin Jesionek

Additional information is available at the end of the chapter

<http://dx.doi.org/10.5772/52590>

---

## 1. Introduction

Since the discovery by S. Iijima in 1991 [1] various potential applications have been proposed for carbon nanotubes (CNTs): sensors, field emission displays, nanometer-sized semiconductor devices and hydrogen storage media. There is a huge literature stream related to nanotube research. On a fundamental level, there are still challenges to mass-produce controlled nanostructures at reasonable cost and new features. There is also a great demand for control versatile electronic characteristics of CNTs. One strategy is to use the CNTs themselves, controlling useful properties *via* their radii and morphologies. An alternative approach leading to new features of CNTs, i.e. directional action on their versatile electronic characteristics, is based on filling them with condensed substances from a wide range of materials [2-8]. CNTs are  $sp^2$  graphene carbon cylinders capable of hosting a variety of species, including 1D crystals of metals, metal salts and oxides; semiconductors; superconductors; and chains of fullerene or endofullerene molecules (see Refs. cited in [7,8]). Such objects are distinguished in their unique physical and chemical properties from both hollow nanotubes and the encapsulated substances, which permits one to purpose-tailor "nanowires" and "nanotubes" with unique physical and chemical properties.

Among materials encapsulated within CNTs are both elementary substances and the binary compounds formed from the group 15–16–17 elements. Figure 1 presents a typical high resolution transmission electron microscopy (HRTEM) image of single-walled carbon nanotube (SWNT) filled with one of the metal halogenides, i.e.,  $BaI_2@SWNT$ . However, one should note the possible filling of SWNTs with the alone helical iodine chains (Figure 2). Of course, the multi-walled carbon nanotubes (MWNTs) can be filled with the elemental forms (e.g., Bi, Sb, S, Se, Te,  $I_2$ ), halogenides (e.g., consistent of Cl, Br,  $I_2$ ), oxides (e.g.,  $Sb_2O_3$ ), and chalcogenides (e.g.,  $Sb_2S_3$ , CdS, SnSe, SnTe, HgTe), too. A comprehensive list of such carbon nanostructures has been reviewed by A. Eliseev et al. [7] and P. Lukanow et al. [8].

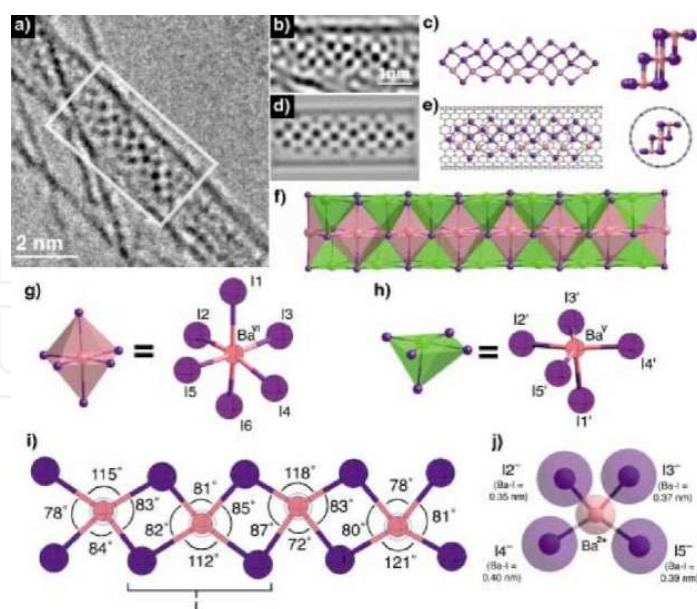


**Figure 1.** a) HRTEM image of  $\text{BaI}_2/\text{SWNT}$  composite. b) Detail from boxed region in (a), for which image noise was reduced with a deconvolution filter. c) Structure plot based on a 2D peak-mapping analysis of (b); end-on view on the right. d) Simulated HRTEM image, e) complete structure model of  $\text{BaI}_2/\text{SWNT}$  composite. f) Coordination model of 1D  $\text{BaI}_2$  chain. g) 5-coordinate, h) 6-coordinate  $\text{BaI}_6$  polyhedra and ball-and-stick models derived from (c). i) and j) Models showing derived equatorial bond angles and distances for  $\text{BaI}_4$  units along the center of the 1D  $\text{BaI}_2$  chain (ionic radii in (j) indicated by diffuse spheres) (Reproduced from [9] with permission. Copyright Wiley-VCH Verlag GmbH).

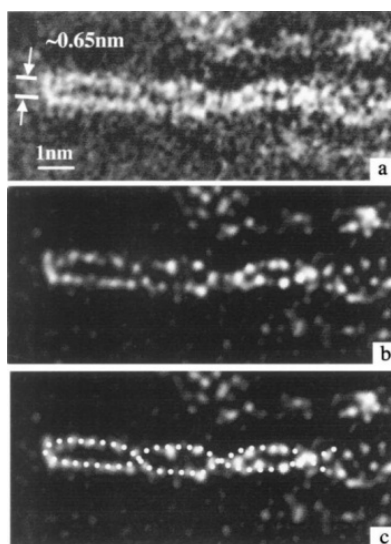


**Figure 2.** a) Higher resolution Z-contrast image of a SWNT containing two strands of iodine. (b) Maximum entropy processed image to reduce the noise. Two constrictions can be seen, consistent with the projection of a double helix configuration with the two chains spiraling along the inside walls of the nanotube as shown in the overlay in (c). The period of the helix is about 5 nm, and the maximum separation of the two strands is  $\sim 0.65$  nm, much less than the 1.3–1.4 nm diameter of the SWNT (Reproduced from [10] with permission. Copyright the American Physical Society).

This review summarizes results of recent investigations [11-14] of carbon nanotubes (CNTs) filled with ternary chalcogenides formed from the group 15–16–17 elements, i.e. antimony sulfide (SbS) and antimony selenide (SbSe) known as SbS-type materials. Some recent original data are presented, too. It should be underlined that the bulk SbS being a semiconducting ferroelectric has an unusually large number of very attractive and suitable properties (see Refs. cited in [15-17]). Among them there are the photoferroelectricity, pyroelectric, pyrooptic, piezoelectric, electromechanical, electrooptic, photorefractive and nonlinear optical effects. Therefore SbS is taken into consideration as a valuable material for many applications (see the literature cited in [15-17]).

SbS type materials have been synthesized in different ways (see Refs. in [15-17]). The most often used method consists in fusion of stoichiometric amounts of antimony, sulfur and iodine or antimony iodide, and antimony sulphide with antimony iodide. The procedure requires high temperature (723 - 873 K) and long reaction time (1-3 days). Recently [15,17], a novel sonochemical method for direct preparation of semiconducting and ferroelectric SbS nanowires has been established. The determined [15,17] value of the indirect forbidden energy band gap of SbS gel  $E_{\text{g,if}}=1.829(27)$  eV is well compared to the bulk value of band gap of SbS reported in the literature (see Refs. in [15,17]). The maximum of dielectric constant  $\epsilon=1.6 \cdot 10^4$  of SbS nanowires was observed at Curie temperature  $T_c=292(1)$  K [17,18] that well corresponds with the phase transition in bulk SbS crystals. It should be underlined that SbSe can be sonochemically prepared in the form of crystalline nanowires [17,19], too.

## 2. Preparation of SbS@CNTs and SbSe@CNTs

There are known a few methods for filling CNTs with different substances [4,6-8]: catalytic synthesis of nanotubes using the metals as catalysts, capillary drawing-in of molten materials or materials dissolved in solvents having a low surface tension, saturation with metal vapor as well as electrochemical methods based on passing the electrical current through an electrolyte containing dissolved metal atoms. In this paper we present another method for inserting materials into the inner cavity of a nanotube. Our method is based on sonochemistry. It is well known [20-25] that ultrasound can induce new reactivities leading to the formation of unexpected chemical species. What makes sonochemistry unique is the remarkable phenomenon of cavitation [25,26]. Comparing sonochemical method of preparing materials with the traditional ones, it can be seen that ultrasound irradiation can be used at room temperature and ambient pressure to promote heterogeneous reactions that normally occur only under extreme conditions of hundreds of atmospheres and degrees (e.g., [20-22]).

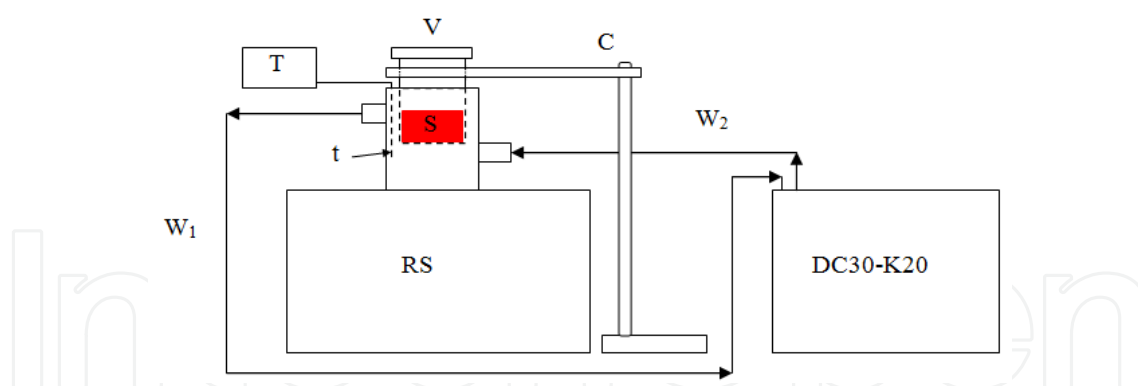


**Figure 3.** Schematic illustration of the set-up for ultrasonic filling of CNTs with SbSI and SbSeI (RS– ultrasonic reactor; DC30-K20 – refrigerated circulator bath;  $W_1$ ,  $W_2$  – thermal cycle; C – stand; S –sample; V – Pyrex glass cylinder; T – temperature controller; t – temperature sensor) [13].

Both SbSI and SbSeI were prepared in CNTs ultrasonically from the constituents (the elements Sb, I, and S or Se) [11–14]. Methanol and ethanol served as the solvents for these reactions, respectively. All the reagents used in experiments were of analytical purity and were used without further purification. Antimony (99.95 %), selenium (99.5 %) and multi-walled CNTs (659258–10G, 90+%) were purchased from Sigma–Aldrich. Sublimated sulfur (pure p.a.), iodine (pure p.a.), absolute methanol (pure p.a.), and absolute ethanol (pure p.a.) were purchased from POCH S.A. (Gliwice, Poland). In a typical procedure of fabrication SbSI@CNTs [11], the elemental mixture with stoichiometric ratio of e.g. 0.380 g Sb, 0.099 g S and 0.394 g I, was immersed with 0.282 g of CNTs in 40 ml absolute methanol, which was contained in a 54 ml Pyrex glass cylinder of 20 mm inside diameter. In the first procedure of fabrication SbSeI@CNTs [14], the elemental mixture with stoichiometric ratio of e.g. 0.156 g Sb, 0.101 g Se and 0.165 g I<sub>2</sub>, was immersed with 0.102 g of CNTs in 10 ml absolute ethanol, which was contained in a 54 ml Pyrex glass cylinder of 20 mm inside diameter. Furthermore, the syntheses of SbSeI in CNTs have been done in [14] for twice and four times greater contents of Se in the mixture (the obtained products are discussed in the next section). Vessels with the substrates were closed during experiments [11, 14] to prevent volatilization of the precipitants in long time tests. Bottoms of the vessels were planar or semispherical and 1 mm in thickness. Figure 3 presents scheme of the technological set-up. The cylinders were partly submerged in water in an ultrasonic reactor (InterSonic IS–UZP–2, frequency 35 kHz, with 75 W electrical power and 2.6 W/cm<sup>2</sup> power density guaranteed by the manufacturer). Temperature of the bath was established using the Haake DC–K20 refrigerated circulator bath (Thermo Scientific). The sonochemical processes were continued for 3 h at 323 K temperature of the water in the ultrasonic reactor. During the sonications sols were formed. It was observed that the color of the suspension changed gradually indicating the growth process of the SbSI and SbSeI. To control this process, measurements of optical diffusive reflectance  $R_d(\lambda)$  of the sample were performed (Figure 4). It was assumed that the sonochemical process is finished when the spectral characteristics of  $R_d(\lambda)$  do not change with time.

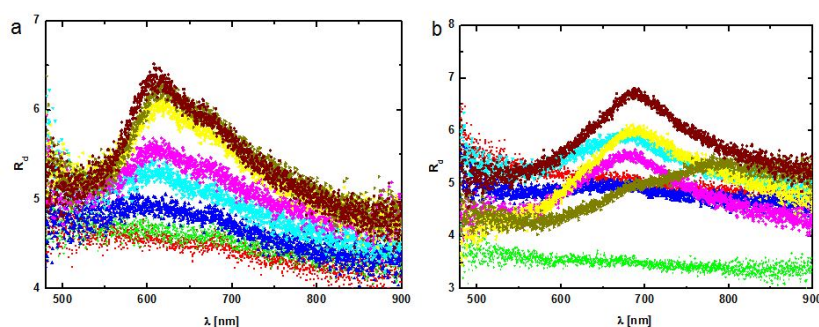


**Figure 4.** Change of diffuse reflectance during the sonication of Sb, S and I in methanol (a) and of Sb, Se and I in ethanol (b) (■ – after 5 min. of sonication,  $T=323$  K; ● – 20 min. ▲ – 40 min. ▼ – 60 min.; ◆ – 80 min.; ◀ – 120 min.; ▶ – 180 min.; ◆ – after washing) [13].

When the sonication processes were finished, a dark sols were obtained. They were centrifuged using the MPW–223e centrifuge, MPW Med. Instruments (Poland), to extract the products. Then the liquids above the sediments were replaced with pure methanol or ethanol to wash the precipitates in the cases of SbSI@CNTs and SbSeI@CNTs, respectively. The centrifugation and washing were performed 5 times in both cases. At the end methanol as well as ethanol were evaporated from the samples during the drying in air at room temperature, so a brown-purple (Figure 5a) and dark brown–purple (Figure 5b) substances were obtained in the cases of SbSI@CNTs and SbSeI@CNTs, respectively.

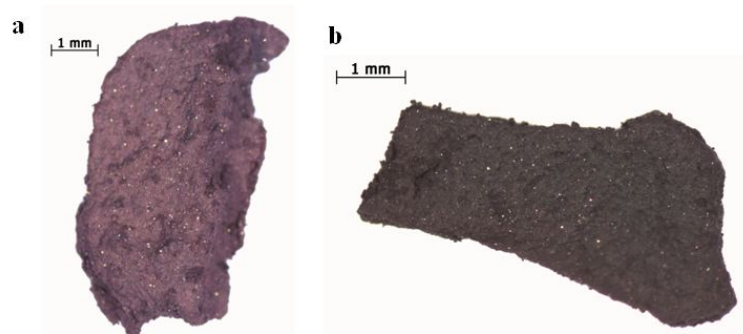


**Figure 5.** Dried MWCNTs filled ultrasonically with SbSI in methanol and SbSeI in ethanol [13].

### 3. Morphology, composition and crystal structure of SbSI@CNTs and SbSeI@CNTs

Characterization of the multi-walled CNTs filled with SbSI or SbSeI [11-14] was accomplished using different techniques, such as powder X-ray diffraction (XRD) performed on a JEOL JDX-7S X-ray diffractometer with graphite monochromatized  $\text{Cu K}\alpha$  radiation ( $\lambda = 0.154056$  nm), scanning electron microscopy (SEM) and energy dispersive X-ray spectroscopy (EDS) performed on a Hitachi S-4200 microscope with EDS Thermo Scientific spectrometer, high-

resolution transmission electron microscopy (HRTEM) and selected area electron diffraction (SAED) performed on a JEOL-JEM 3010 microscope.

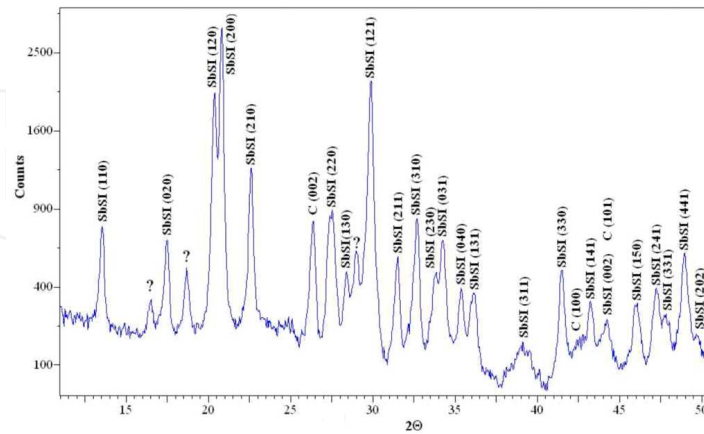


**Figure 6.** The powder XRD pattern of dried CNTs filled with SbSI ultrasonically in methanol [11].

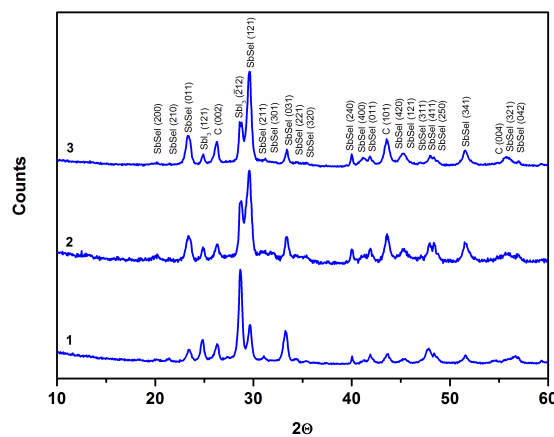


**Figure 7.** The powder XRD patterns of dried multi-walled CNTs filled with SbSeI ultrasonically in ethanol with different compositions of the reactants [14] (1- 0.101 g Se, 2- 0.202 g Se, 3- 0.404 g Se; 0.156 g Sb, 0.165 g I<sub>2</sub>, and 0.102 g of CNTs in 10 ml absolute ethanol; described peaks correspond to the crystalline SbSeI [27,28], C [29,30] and SbI<sub>3</sub> [31,32]).

The powder XRD pattern of the MWNTs filled with SbSI is shown in Figure 6. The well-defined, sharp diffraction lines suggest the well-crystallized substance. It was found that the diffraction lines can be divided into three groups. In the first group, containing most of the lines, the peaks can be indexed to be a pure orthorhombic phase for SbSI with the cell constants  $a=0.858$  nm,  $b=1.017$  nm, and  $c=0.414$  nm. The identification was done using the PCSI-WIN computer program and the data from JCPDS-International Centre for Diffraction Data 2000. The intensities and positions of the peaks are in good agreement with literature values for SbSI [33]. The second group of diffraction lines can be indexed to be a carbon phase P6<sub>3</sub>mc with the cell constants  $a=0.2470$  nm and  $c=0.6790$  nm [30]. The third group of a few addition-

al X-ray diffraction lines for  $2\theta$  equal  $16.51^\circ$ ,  $18.66^\circ$  and  $29.00^\circ$  has given the following values of  $d_{hkl}$ : 0.536 nm, 0.475 nm, and 0.308 nm, respectively. These lines may be explained as follows. The XRD investigations [34] of SbSI sonochemically produced in methanol show the coexistence of phases with  $Pna2_1$  and  $Pnam$  crystal symmetry that are characteristic for ferroelectric and paraelectric domains, respectively. Hence, such data obtained at 298 K represent a structure of just below or very near the transition temperature of SbSI. Another explanation for the additional X-ray diffraction lines can be given taking into account existence of unknown phase in the investigated material. This problem must be studied in the future.

XRD	SAED	HRTM	Literature data									
			C [30]		SbSeI [28]		SbI <sub>3</sub> [32]					
$2\theta$	$I_{rel}$	$d_{hkl}$ [pm]	$d_{hkl}$ [pm]	hkl	sign	$d_{hkl}$ [pm]	$d_{hkl}$ [pm]	hkl	$d_{hkl}$ [pm]	hkl	$d_{hkl}$ [pm]	hkl
20.166	8	440.0			2	432(13)			434.9	200		
21.468	8	413.6							401.3	210		
23.324	35	381.1							383.66	011		
24.961	17	356.4									351.41	121
26.245	29	339.3			1	332(5)	339.5	002				
28.797	49	309.8									311.63	$\bar{2}12$
29.602	100	301.5							303.13	121		
31.183	13	286.6							287.7	211		
31.768	10	281.4							279.3	301		
33.422	22	267.9							265.62	031		
34.488	9	259.8							259.51	221		
35.457	8	253.0							253.3	320		
40.013	17	225.1	223.35	$2\bar{4}0$					223.35	240		
41.154	13	219.2							217.45	400		
41.869	15	215.6					213.9	100	215.88	321		
43.578	32	207.5	206.35	002			204.02	101	206.35	002		
45.117	17	200.8							200.65	420		
45.448	17	199.4							197.14	112		
47.029	8	193.1							195.85	331		
47.966	15	189.5							189.17	411		
48.459	13	187.7							187.81	250		
51.546	21	177.2							175.3	341	177.12	143
54.88	8	167.2					169.75	004				
55.806	14	164.6							165.9	321		
56.981	10	161.5							161.7	042		
			151.56	$\bar{2}42$					151.56	242		

**Table 1.** Comparison of interplanar spacings determined by XRD (Figure 7), SAED (Figure 14) and HRTEM (Figure 12) of multi-walled CNTs filled with SbSeI sonochemically in ethanol with literature data for CNTs, SbSeI orthorhombic crystals, and SbI<sub>3</sub> monoclinic crystals.

The powder XRD patterns of the CNTs filled ultrasonically with SbSeI are shown in Figure 7. One can see that the best results (the lowest intensity of  $\text{SbI}_3$  peaks) have been obtained for four times greater content of Se in the mixture (compare curves in Figure 7). These results indicate that the CNTs should be filled with SbSeI with the excess of Se. The well-defined, sharp diffraction lines suggest the well-crystallized substance (curve 3 in Figure 7). It was found that the diffraction lines can be divided into three groups (Table 1). In the first group, containing most of the lines, the peaks can be indexed to be a pure orthorhombic phase for SbSeI with the cell constants  $a=0.8698$  nm,  $b=1.0412$  nm, and  $c=0.4127$  nm [27,28]. The intensities and positions of the peaks are in good agreement with literature values for SbSeI [27,28]. The second group of diffraction lines can be indexed to be a carbon phase  $P6_3mc$  with the cell constants  $a=0.2470$  nm and  $c=0.6790$  nm [29,30]. The third group of a few additional X-ray diffraction lines can be attributed to the monoclinic antimony iodide ( $\text{SbI}_3$ ) with the cell constants  $a=0.7281$  nm,  $b=1.0902$  nm,  $c=0.8946$  nm, and  $\beta=109.930^\circ$  [31,32]. It can be explained as follows. In ethanol iodine reacts with antimony forming antimony iodide (1). This substance is soluble in alcohols [35]. When the alcohol is evaporated, the  $\text{SbI}_3$  crystallizes. It is probable that (despite the washing of the CNTs sonochemically filled with SbSeI) some portion of  $\text{SbI}_3$  still exists in the product. This problem should be solved in the future.

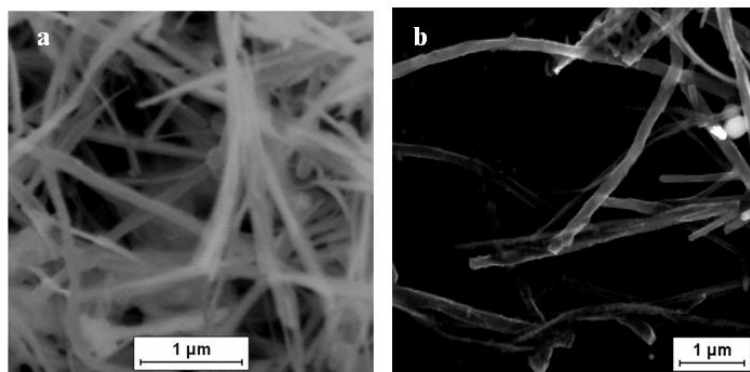


**Figure 8.** The typical SEM micrographs of dried gels of SbSI@CNTs [11] and SbSeI@CNTs [14].

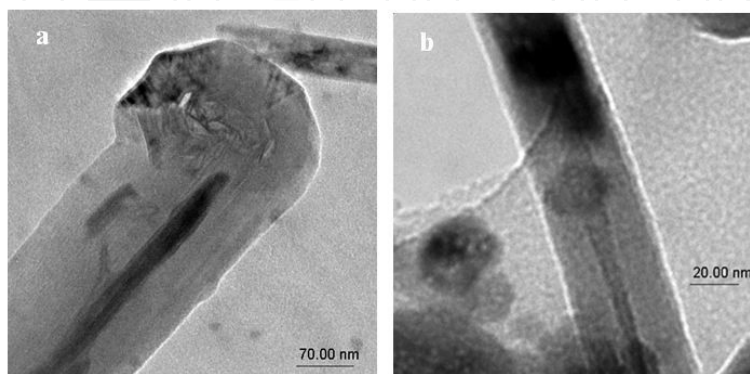


**Figure 9.** Typical TEM images of an individual SbSI@CNT [11] and SbSeI@CNT [14].

The typical SEM micrographs of the dried SbSI@CNTs and SbSeI@CNTs prepared sonochemically in methanol and ethanol, respectively, are shown in Figures 8 and 9. The samples used for SEM and EDS observations were prepared by dispersing a small quantity of the CNTs filled with SbSI or SbSeI in ethanol followed by ultrasonic vibration for 10 min. One or two drops of the nanoparticle solutions were deposited on naturally oxidized silicon single crystal plate and dried in 120 min at room temperature in vacuum. One can see SbI<sub>3</sub> nanoparticles around some of the SbSeI@CNTs (Figure 9). Probably, these nanoparticles have been grown from the solution (SbI<sub>3</sub> dissolved in ethanol) during drying of the product. The SbI<sub>3</sub> by-product is the rest of intermediate compound obtained during sonochemical synthesis of SbSeI [36]. The dimension of SbI<sub>3</sub> nanoparticle has been about 30 nm. The chemical composition and crystal structure of these nanoparticles have been proved [14].

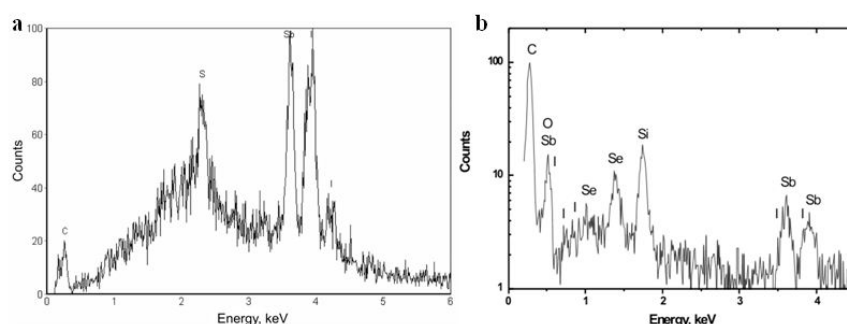


**Figure 10.** The EDS spectra of dried multi-walled CNTs filled ultrasonically with SbSI [11] and SbSeI [14] (the investigated material was deposited on naturally oxidized Si single crystal).

Results of EDS investigations				
Element	SbSI@CNTs [11]		SbSeI@CNTs [14]	
	Concentration of all detected elements (at. %)	Concentration of components without C (at. %)	Concentration of components without Si and O (at. %)	Concentration of components without Si, O and C (at. %)
Sb	5.1(3)	46(2)	2.1	44
S	1.7(3)	21(3)	–	–
Se	–	–	1.3	28
I	3.8(3)	33(2)	1.3	28
C	89.4(13.4)	–	95.3	–

**Table 2.** Atomic concentration of components determined by EDS of the multi-walled CNTs filled sonochemically with SbSI in methanol and with SbSeI in ethanol.

The EDS spectra of dried multi-walled CNTs filled ultrasonically with SbSI and SbSeI are presented in Figure 10. The measured atomic concentrations of Sb, S, Se, I and C (without Si and O from the supporting wafer) are presented in Table 2. Taking into consideration the large excess of Sb and the deficit of S or Se as well as I detected by EDS, it should be underlined that the EDS analysis performed on sonochemically produced alone SbSeI gel confirmed an elemental atomic ratio of 0.41:0.26:0.33 for Sb, Se, and I [19]. Therefore, as it was suggested in [19], probably a separate phase of Sb and I is present, and presumably it is adsorbed on the surface of the SbSeI. A similar case was recently discovered in the XPS investigations of sonochemically prepared SbSI nanowires [37]. It is improbable that the excess Sb is present within the ordered SbSI and SbSeI nanowires inside the CNTs, since the interplanar spacings corresponds to stoichiometric materials (Figures 11 and 12). In [37] the antimony subiodide was suggested as the hypothetical material of the surface layer on SbSI nanowires. Such  $Sb_3I$  subiodide was obtained sonochemically [38]. Probably, there is the same compound on the surface of sonochemically prepared SbSeI nanowires. The existence of this substance will be investigated in the near future.

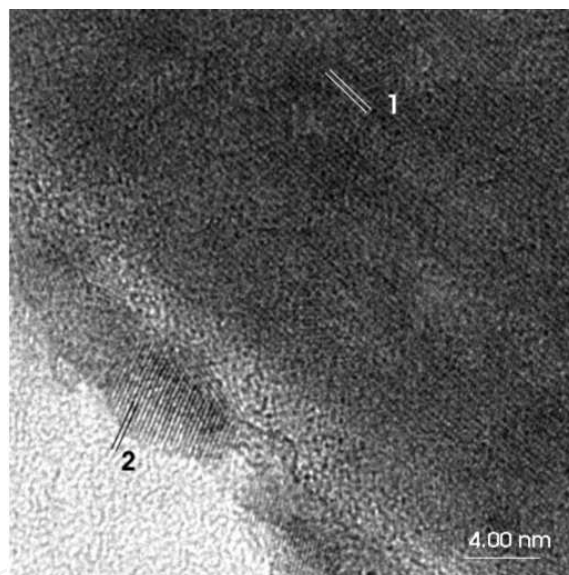


**Figure 11.** HRTEM image of an individual MWCNT filled with SbSI sonochemically in methanol. The fringe spacings of 0.319(2) nm (1) and 0.209(2) nm (2) correspond to the interplanar distances between the (220) planes of SbSI crystal and (101) planes of carbon nanotube, respectively [11].

The TEM (Figure 9) and HRTEM images (Figures 11 and 12) of an individual CNTs sonochemically filled with SbSI and SbSeI reveal that the products consist of coaxial nanocables. The lateral dimensions of the SbSI@CNTs and SbSeI@CNTs have been in the ranges from 30 to 200 nm and from 20 to 170 nm, respectively [11,14]. Lengths of these nanocables reach up to several micrometers in both cases. The HRTEM images of individual CNTs sonochemically filled with SbSI (Figure 11) exhibit good crystallinity of the SbSI and its clear (220) lattice fringes parallel to the nanocable axis. It indicates the growth of SbSI inside the CNT in [001] direction. The interplanar spacing is about 0.319(2) nm, which coincide with the interplanar

spacing 0.32494 nm of (220) planes of the orthorhombic structure of conventional SbSI [33]. Figure 11 shows also the lattice fringes of the CNT walls. The fringe spacings of 0.209(2) nm match with the 0.21390 nm interplanar distances between the (101) planes of carbon nanotubes [30]. All these results correspond well with the XRD patterns (Figure 6) of the CNTs sonochemically filled with SbSI. The SAED pattern (Figure 13) recorded on the end of multi-walled CNT filled with SbSI (presented in Figure 9a) indicates the interplanar spacings appropriate for CNTs as well as SbSI crystals (see Table 3).

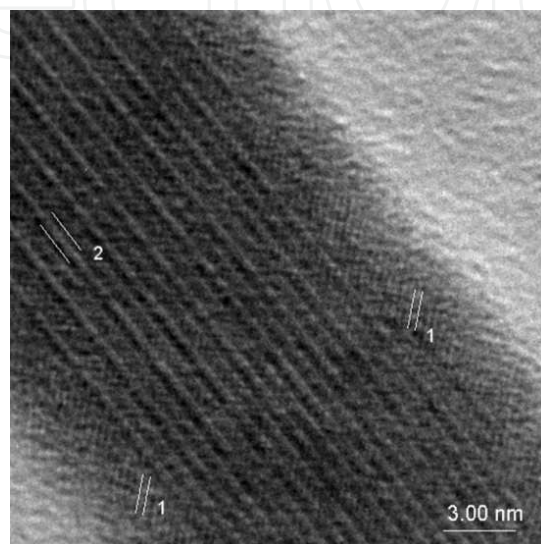


**Figure 12.** HRTEM image of an individual multi-walled CNT filled with SbSI sonochemically in ethanol. The fringe spacings of 0.332(5) nm (sign 1) and 0.432(13) nm (sign 2) correspond to the interplanar distances between the (002) planes of carbon nanotube and (200) planes of SbSI crystal, respectively [14].

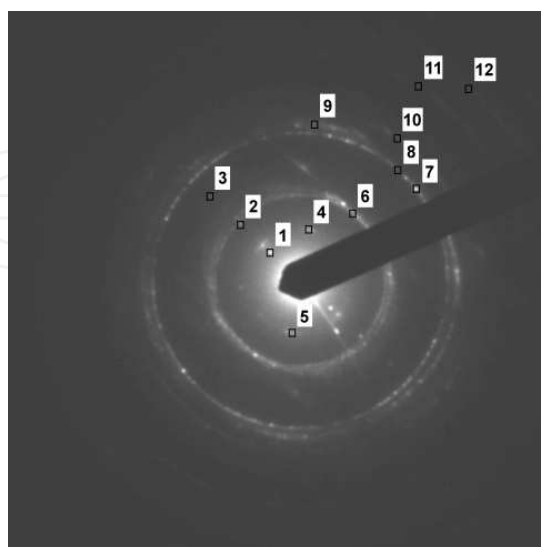


**Figure 13.** SAED pattern of MWCNT filled with SbSI ultrasonically in methanol [11] (shown in Figure 9). The diffraction patterns correspond to the interplanar distances presented in Table 3.

Sign	Results of the SAED $d_{hkl}$ (nm)	Literature data			
		for C [29, 30]		for SbSI [27, 33]	
		$d_{hkl}$ (nm)	(hkl)	$d_{hkl}$ (nm)	(hkl)
1 reflex	0.4360	–	–	0.43402	(120)
		–	–	0.42450	(200)
4 reflex	0.3732	–	–	0.38465	(011)
5 reflex	0.3470	0.33950	(002)	0.35036	(111)
2 reflex	0.2189	0.21390	(100)	0.21663	(330)
6	0.2089	0.20402	(101)	0.20800	(002)
3 reflex	0.1446	–	–	0.14244	(422)
		–	–	0.14244	(531)
7 reflex	0.1190	–	–	0.12031	(143)
		–	–	0.11960	(181)
8 circle	0.1210	0.12350	(110)	–	–
9 circle	0.1155	0.11606	(112)	–	–
		0.11464	(105)	–	–
		0.11316	(006)	–	–
10 circle	0.1036	0.10425	(202)	–	–
11 circle	0.07874	0.07954	(122)	–	–
12 circle	0.07038	0.07720	(206)	–	–

**Table 3.** Comparison of interplanar spacings determined by SAED (Figure 13) of multi-walled CNT filled with SbSI ultrasonically in methanol with literature data for CNTs and SbSI bulk crystals.

The HRTEM images of an individual CNTs sonochemically filled with SbSeI (Figure 12) exhibit good crystallinity of the SbSeI and its clear (200) lattice fringes parallel to the nanocable axis. It indicates the growth of SbSeI inside the CNT in [001] direction. The interplanar spacing is about 0.432(13) nm, which coincide with the interplanar spacing 0.4349 nm of (200) planes of the orthorhombic structure of conventional SbSeI [28]. Figure 12 shows also the lattice fringes of the CNT walls. The fringe spacings of 0.332(5) nm match with the 0.3395 nm interplanar distances between the (002) planes of carbon nanotubes [30]. All these results correspond well with the XRD patterns (Figure 7, Table 1) of the CNTs sonochemically filled with SbSeI. The SAED pattern (Figure 14) recorded on the multi-walled CNT filled with SbSeI (presented in Figure 12) indicates the interplanar spacings appropriate for SbSeI crystals (see Table 1). Surprisingly, the presence of SbSeI nanowires or SbSeI material on the outer walls of the MWCNT has not been observed in the HRTEM and TEM images. Probably, the process of capillary suction of molecules into carbon nanotubes facilitates the process of SbSeI nanocrystal growth.

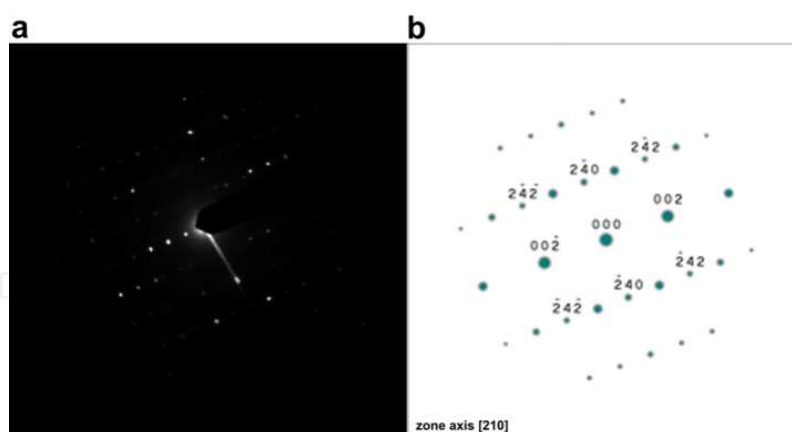


**Figure 14.** Electron diffraction pattern of multi-walled CNT filled with SbSeI ultrasonically in ethanol [14] in the orientation close to the [210] zone axis (a) and its simulated diagram (b). The diffraction patterns correspond to the interplanar distances presented in Table 1.

#### 4. Mechanisms of sonochemical preparation of SbSI@CNTs and SbSeI@CNTs

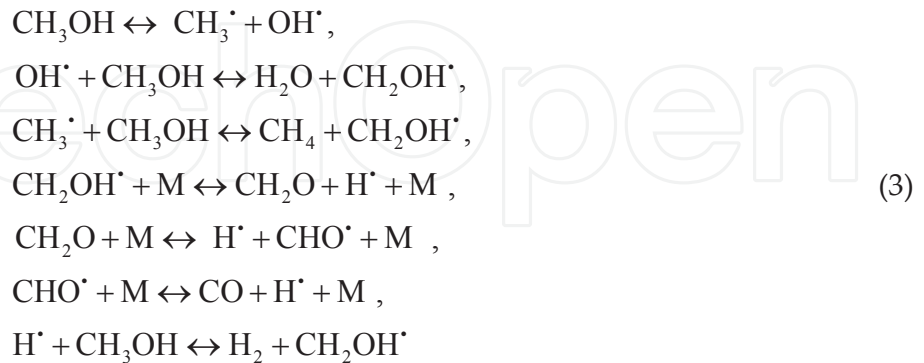
It is known that the mode of insertion dictates the nature and morphology of the obtained filling of CNTs [39]. When the filling is induced via solution-deposition, small discrete encapsulates are obtained, whereas when it is obtained via capillarity, continuously filled CNTs are observed. Probably the last happens when CNTs are filled sonochemically by SbSI [11] as well as by SbSeI [14]. As in the case of sonochemically produced alone SbSI [15] and SbSeI [19], the transient high-temperature and high-pressure field produced during ultrasound irradiation provide a favorable environment for the 1D growth of the SbSI and SbSeI nanocrystals from elements inside multi-walled CNTs in ethanol, though the bulk solution surrounding the collapsing bubbles is at relatively low temperature ( $T=323$  K) and atmospheric pressure.

The probable reaction routes of synthesis of SbSI and SbSeI in CNTs, and the mechanisms of nanowires formation using elemental Sb, S or Se and I in the presence of methanol and ethanol under ultrasonic irradiation can be summarized as follows:

- a. iodine,  $I_2$ , dissolved in methanol or ethanol reacts with antimony and forms the antimony triiodide,  $SbI_3$ , also dissolved in ethanol [40]



- b. dehydrogenation, dehydration as well as decomposition of ethanol (2) and methanol (3) in or close to the cavitation bubbles leads to the formation of hydrogen and water [41,42]



- c. the sonolysis of water yields the  $\text{H}^\bullet$  and  $\text{OH}^\bullet$  radicals



- d. the ultrasonic irradiation facilitates the reduction of chalcogens to the active forms of  $\text{S}^{-2}$  and  $\text{Se}^{-2}$  (see Refs. in [24,43]) that react with the in-situ generated  $\text{H}^\bullet$  radicals forming  $\text{H}_2\text{S}$  and  $\text{H}_2\text{Se}$  [44]



- e. opening of the CNT ends due to the acids ( $\text{H}_2\text{S}$ ,  $\text{H}_2\text{Se}$ ) [7] or the action of ultrasounds [45,46].
- f. CNT's suck the released  $\text{H}_2\text{S}$  or  $\text{H}_2\text{Se}$  molecules and  $\text{SbI}_3$  in ethanol needed to build  $\text{SbSI}$  and  $\text{SbSeI}$ . This is allowed by the capillary effect [47]. It is well known [48,49], that open CNTs are impregnated with excess of the precursor solutions under ultrasonic conditions to ensure that most of the tubes can be filled by the impregnating solution. From the thermodynamic point of view, the dissolution of the impregnating solution sticking to external walls of CNTs into the washing medium necessitates the condition of the solvation energy gain smaller than zero [48,49]. On the other hand, the energy gain for the capillary filling of a CNT must be smaller than the solvation energy to ensure that the solution is stable in the internal cavity of CNTs [48,49].
- g.  $\text{H}_2\text{S}$  or  $\text{H}_2\text{Se}$  reacts with  $\text{SbI}_3$  to yield  $\text{SbSI}$  and  $\text{SbSeI}$  molecules



- h. SbSI or SbSeI molecules, under the microjets and shockwaves formed during collapsing of the bubbles, are pushed towards each other in CNTs and are held by chemical forces. Therefore, the nuclei of SbSI or SbSeI are formed as a result of the interparticle collisions (see [24]).
- i. the freshly formed nuclei in the solution are unstable and have the tendency to grow into double chains  $[(\text{SbSI})_\infty]_2$  or  $[(\text{SbSeI})_\infty]_2$  consisting of two chains related by a twofold screw axis and linked together by a short and strong Sb-S or Sb-Se bonds [50]. Local turbulent flow associated with cavitation and acoustic streaming greatly accelerates mass transport in the liquid phase;
- j. the SbSI and SbSeI chains can be readily crystallized into a 3D lattice in the CNTs through van der Waals interactions. Induced by this structure, crystallization tends to occur along the c-axis, favoring the stronger covalent bonds over the relatively weak, inter-chain van der Waals forces [51]. Thus, this solid material has a tendency to form highly anisotropic, 1D structures also inside the CNTs.

The (7) and (8) were the basic reactions used in different methods of preparation of bulk SbSI-type crystals [52]. Despite the tubes filling, the observed nanowire type morphology of the product (Figures 11 and 12) is possibly due to the inherent chain type structure and growth habit of the SbSI as well as SbSeI crystals [50].

## 5. Optical properties of SbSI@CNTs and SbSeI@CNTs

Optical absorption spectra have been extensively used as one of the most important tools for probing the energy gaps ( $E_g$ ) and band structures of semiconductors [53]. There are several methods for measuring them. These include diffuse reflectance spectroscopy (DRS). When a material, consisting of many particles or nanoparticles, is illuminated some of the impinging radiation penetrates the sample and some is reflected from its surface. The portion that penetrates the sample is scattered at a large number of points in its path as well as it is transmitted through the particles a number of times. Only the part of this radiation that is returned to the surface of the sample and comes back out is considered to be diffuse reflection. This component has been investigated extensively by many authors [54-56]. DRS is a suitable, not destructive, and simple method of investigation, especially important in examinations of porous, nanocrystalline materials and gels [57]. It is impossible to examine such materials applying specular reflection and it is also extremely difficult to determine the pathlength in an optical transmittance of them. The following factors are related to high spectral quality of diffuse reflectance:

1. dilution of the sample with a non-absorbing matrix ensures a deeper penetration of the incident beam into the sample which increases the contribution of the scattered component in the spectrum and minimizes the specular reflection component;
2. smaller particles improve the quality of DRS spectra because the contribution of reflection from the surface is reduced.

The optical diffuse reflection spectroscopy (DRS) of SbSI@CNTs and SbSeI@CNTs was carried out [11,14] on a spectrophotometer SP-2000 (Ocean Optics Inc.) equipped with an integrating sphere ISP-REF (Ocean Optics Inc.). Spectra were recorded at room temperature, from 350 to 1000 nm. The standard WS-1 (Ocean Optics Inc.) was used as a reference. The diffuse reflectance values were converted to the Kubelka–Munk function (known to be proportional to the absorption coefficient) shown by [54-56]

$$F_{K-M}(R_d) = \frac{(1 - R_d)^2}{2R_d} \sim \alpha \quad (9)$$

where  $R_d$  describes the coefficient of diffuse reflectance and  $\alpha$  is the absorption coefficient of light in the investigated material.

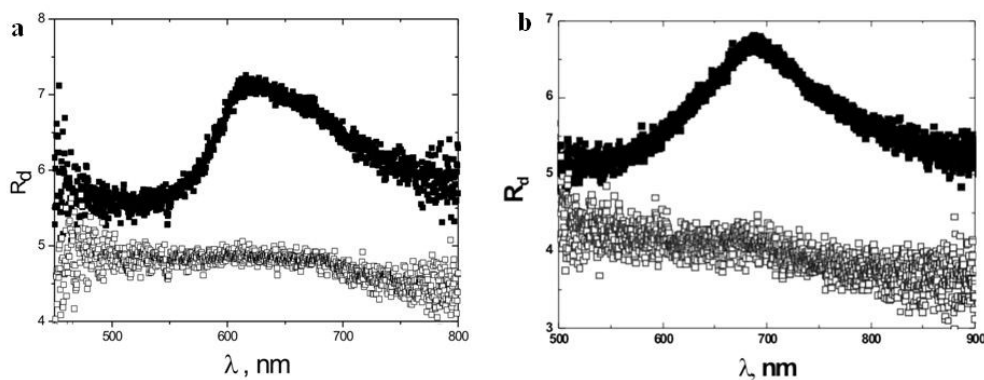


**Figure 15.** Comparison of the diffuse reflectance spectra of the multi-walled CNTs filled with SbSI (a) [11] and SbSeI (b) [14] (■) ultrasonically (in methanol and ethanol, respectively), and of the empty multi-walled CNTs (□) in methanol and ethanol.

In Figure 15 the diffuse reflectance spectra of CNTs filled with SbSI and SbSeI are compared with the spectrum registered for hollow CNTs. In the first cases one can see the characteristic for semiconducting materials edges of fundamental absorption around 615 nm and 687 nm. However, the diffuse reflectance decreases also with increasing wavelengths (Figure 15), probable due to the large amount of free carriers absorbing light. Figure 16 presents the spectra of Kubelka–Munk functions derived from the diffuse reflectance data presented in Figure 15.

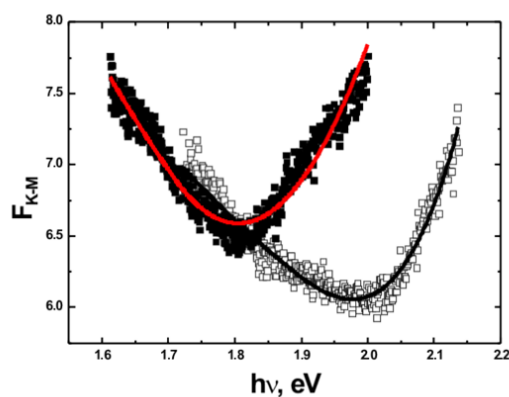


**Figure 16.** Comparison of fitted spectra of Kubelka–Munk functions calculated for diffuse reflectances of multi-walled CNTs filled with SbSel (■) with the data reported for multi-walled CNTs filled with SbSI (□). Solid curves represent the least square fitted theoretical dependences (description in the text; values of the fitted parameters are given in Table 4) [14].

Fitted parameters	CNTs filled with SbSel [14]			SbSel nanowires [19]	CNTs filled with SbSI [11]	SbSI nanowires [57]
	Values determined assuming					
	Indirect allowed absorption	Indirect allowed absorption without phonon statistics – normalized for hv	Indirect forbidden absorption			
$\chi^2$	0.1223	5.592	78.14	–	–	–
$E_{\text{gif}}$ [eV]	–	–	1.6(1)	1.63	1.871	1.854
$E_{\text{gla}}$ [eV]	1.61(6)	1.72(4)	–	–	–	–
$E_{\text{ph}}$ [eV]	0.099(6)	–	–	–	–	–
$A_{60}$ [1/eV <sup>3</sup> m]	–	–	41(2)	94.8	95.6	157
$A_{123}$ [10 <sup>12</sup> m <sup>-3</sup> ]	11.14(1)	11(2)	11.11(1)	–	8.24	–
$A_{50}$ [1/eV <sup>2</sup> m]	27.7(6)	–	–	–	–	–
A41 [1/eV <sup>2</sup> m]	–	60(1)	–	–	–	–
$A_0$ [1/m]	1.019(1)	1(1)	1.02(2)	0.01071	2.702	0.0213
$E_U$ [eV]	–	–	–	0.0810	–	0.147
$A_U$ [1/m]	–	–	–	1.09·10 <sup>-10</sup>	–	84.4·10 <sup>-9</sup>

**Table 4.** Comparison of parameters of multi-walled CNTs filled with SbSI and SbSel with the literature data reported for SbSel and SbSI nanowires produced sonochemically ( $E_{\text{gla}}$  – indirect allowed energy gap;  $E_{\text{gif}}$  – indirect forbidden energy gap;  $E_{\text{ph}}$  – phonon energy;  $E_U$  – Urbach energy;  $A_0$  – constant absorption;  $A_{50}$ ,  $A_{60}$ ,  $A_{120}$  – proportionality factors determined from the fitting of the spectra of  $F_{\text{K-M}}$  functions evaluated from the DRS data).

The Kubelka–Munk ( $F_{\text{K-M}}$ ) spectra were least square fitted with theoretical dependences appropriate for different mechanisms of absorption [57]. The best fitting was obtained for the

sum of indirect allowed absorption with absorption/emission of phonons ( $\alpha_1$ ), free carrier absorption ( $\alpha_2$ ) and constant absorption term ( $\alpha_3$ ) (see the literature in [53,57]):

$$\alpha = \alpha_1 + \alpha_2 + \alpha_3 \quad (10)$$

where

$$\alpha_1 = A_{50} \frac{(h\nu - E_{gla} + E_{ph})^2}{\exp\left(\frac{E_{ph}}{k_B T}\right) - 1} \quad \text{for} \quad (11)$$

$$E_{gla} - E_{ph} < h\nu \leq E_{gla} + E_{ph}$$

$$\alpha_1 = A_{50} \left\{ \frac{(h\nu - E_{gla} + E_{ph})^2}{\exp\left(\frac{E_{ph}}{k_B T}\right) - 1} + \frac{(h\nu - E_{gla} - E_{ph})^2}{1 - \exp\left(-\frac{E_{ph}}{k_B T}\right)} \right\} \quad (12)$$

*for*  $h\nu > E_{gla} + E_{ph}$

$$\alpha_2 = A_{123} \cdot \lambda^2 \quad (13)$$

$$\alpha_3 = A_0 \quad (14)$$

$E_{gla}$  represents the indirect allowed energy gap,  $E_{ph}$  is the phonon energy,  $A_0$ ,  $A_{50}$ ,  $A_{123}$  are constant parameters,  $h\nu$  is the photon energy,  $T$  is the temperature,  $k_B$  is the Boltzmann constant. The determined values of these parameters are given in Table 4. In the same table they are compared with the literature data reported for SbSeI [19] and SbSI [57] nanowires produced sonochemically.

It should be noted that absorption spectra [58-62] of bulk SbSeI single crystals have been fitted as indirect allowed absorption without phonon statistics – normalized for  $h\nu$  ( $\alpha_4$ )

$$\alpha_4 = \frac{A_{41}}{h\nu} (h\nu - E_{gla})^2 \quad \text{for } h\nu > E_{gla} \quad (15)$$

where  $E_{gla}$  represents the indirect allowed energy gap,  $A_{41}$  is the proportionality factor. It should be noted that the indirect allowed optical energy gap described by formulae (17) was discovered also in doped single crystals SbSeI:Co [61], SbSeI:V [60], SbSeI:Cr [59], and

SbSeI:Ni [58]. Therefore, we fitted the same spectrum of  $F_{K-M}$  of the CNTs filled with SbSeI (Figure 16) with theoretical dependence appropriate for the sum of indirect allowed absorption without phonon statistics – normalized for  $h\nu$  ( $\alpha_4$ ), free carrier absorption ( $\alpha_2$ ) and constant absorption term ( $\alpha_3$ ). Values of the fitted parameters are given in Table 4, too. However, the value of sum of squared residuals ( $\chi^2$ ) in the last fitting is over six hundred times larger than in the case of fitting with formula (10) (Table 4).

One should remember that the  $F_{K-M}$  spectrum of sonochemically produced alone SbSeI nanowires [19] was best fitted for indirect forbidden absorption ( $\alpha_5$ ), Urbach ruled absorption ( $\alpha_6$ ) and constant absorption term ( $\alpha_3$ ), where

$$\alpha_5 = A_{60} (h\nu - E_{gff})^3 \quad \text{for } h\nu > E_{gff} \quad (16)$$

$$\alpha_6 = A_U \exp \left[ \frac{h\nu}{E_U} \right] \quad (17)$$

Therefore, we fitted the same spectrum (Figure 16) of  $F_{K-M}$  of the CNTs filled with SbSeI with theoretical dependence appropriate for the sum of  $\alpha_5$ ,  $\alpha_2$  and  $\alpha_3$  (the fitting did not take into account the  $\alpha_6$  because it is in contradiction with the experimental data described by  $\alpha_2$ ). One can see that the value of sum of squared residuals ( $\chi^2$ ) in the last fitting is over forty five times larger than in the case of fitting with the indirect allowed absorption (Table 4).

The observed free carrier absorption of light in the case of CNTs filled with SbSI and SbSeI is evoked by the CNTs material because it is absent in the case of alone SbSI and SbSeI nanowires [19,57]. Instead of it the Urbach absorption was reported in the latter cases. May be the latter mechanism of absorption exists also in CNTs filled with SbSI and SbSeI but it is hidden by the free carrier absorption. It is known (see [47]) that a metal atom intercalated inside the internal cavity of a CNT displays a tendency towards the transfer of some part of the valence electrons to the outer surface of the nanotube, where unoccupied electronic states exist. As a result of such a transfer there arises an additional mechanism of electrical conduction, related to the travel of an electron about those states.

The nanocrystalline SbSeI filling the CNTs is a semiconductor with little smaller energy gap of 1.61 eV than the alone SbSeI nanowires (Table 4). The established type of indirect allowed energy gap of SbSeI in CNTs is different from the indirect forbidden energy gap of sonochemically produced alone SbSeI nanowires [19]. However, one should remember that absorption spectra [58-62] of bulk SbSeI single crystals have been fitted with indirect allowed absorption without phonon statistics – normalized for  $h\nu$ . Therefore, the indirect allowed energy gap of SbSeI in CNTs is very probable and the light absorption in the alone SbSeI nanowires should be studied again.

## 6. Electrical and photoelectrical properties of SbSI@CNTs and SbSeI@CNTs

In [13] for the first time electrical investigations have been performed on circular samples of SbSI@CNT gel prepared sonochemically. The diameter and thickness of the sample were 4 mm and 1.5 mm, respectively. The largest opposite surfaces of the sample were covered with a silver paste (SPI Supplies) and electrical connection from these electrodes was made by copper wire. The measurements were performed applying impedance analyzer Agilent 4294A in the frequency ( $f$ ) range 200 Hz – 20 MHz with amplitude of 0.01 V and zero bias. The impedance investigations were made in vacuum in the temperature region from 273 K to 353 K using a LN2 cryostat VPF-700 (Janis Research Company, Inc.). The metallic chamber served as a Faraday cage in order to eliminate undesired external interference. The temperature was controlled using 331 Temperature Monitor, (Lake Shore). Measurements were performed in darkness to avoid the excess carriers that can be photogenerated in SbSI@CNT. LabView program has been developed for computer-controlling the experiment, data acquisition and analysis.

Figures 17a and 17b present influence of temperature on Bode plots for SbSI@CNT gel prepared ultrasonically in methanol. The impedance amplitude ( $|Z|$ ) decreases while the phase ( $\phi$ ) increases with increasing frequency. Using formulae:  $\text{Re}Z = |Z| \cos\phi$  and  $\text{Im}Z = |Z| \sin\phi$ , the Nyquist plots (Figure 17c) have been constructed. The two arcs in Nyquist plots, in the temperature range from 273 K to 293 K, suggest the need of using non Debye model to interpret the data. Hence, the equivalent circuit to interpret the impedance of SbSI@CNT gel should contain the constant phase element (CPE) with impedance given by

$$Z_{CPE} = \left[ A(j\omega)^n \right]^{-1} \quad (18)$$

where: parameter  $A$  is a constant,  $j^2 = -1$ ,  $\omega = 2\pi f$ , the exponent  $n$  equals 1 for ideal capacitor, 0.5 in the case of diffusion processes, 0 for ideal resistor, and -1 for ideal inductor [63]. The porous materials have values of  $n$  from the range  $0.9 \div 1$  [63].

For temperatures higher than  $T=293$  K only one arc in Nyquist plots is observed (Figure 17c). Probably, it is evoked by the ferroelectric-paraelectric phase transition of SbSI near Curie temperature  $T_C=292(1)$  K [17,18].

The experimental data have been best fitted (Figure 17) employing complex nonlinear curve fitting using ZView 2 program [64]. Fitting of the Nyquist plots has been done using equivalent circuits reported for different models (e.g. Voigt circuit, Maxwell circuit, and their combinations). The best fitting was obtained using equivalent circuit shown in Figure 18. It is consistent of serial connection of two parallel circuits (resistors:  $R_1$ ,  $R_2$  and CPE elements:  $CPE_1$ ,  $CPE_2$ ) with inductance  $L$ . Probably, the first parallel circuit ( $R_1 - CPE_1$ ) represents properties of SbSI component while the second parallel circuit ( $R_2 - CPE_2$ ) describes properties of CNTs and the electrodes. The inductance  $L$  is dedicated to the presence of CNTs [65,66].

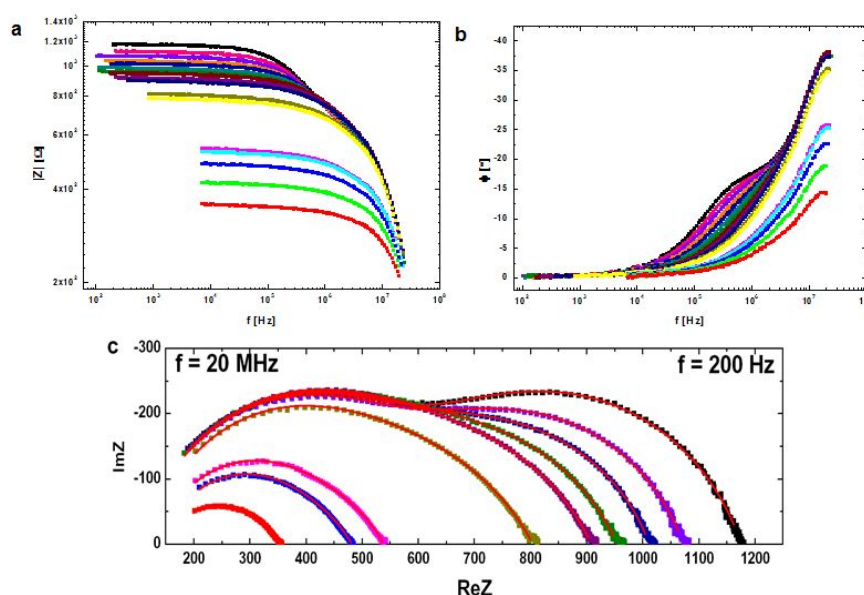


**Figure 17.** Influence of temperature on Bode (a, b) and Nyquist (c) plots for SbSI@CNT gel prepared ultrasonically in methanol [13] (■ – 273 K, ■ – 283 K, ■ – 293 K, ■ – 303 K, ■ – 313 K, ■ – 323 K, ■ – 333 K, ■ – 343 K, ■ – 353 K). Solid curves represent the fitted theoretical dependences calculated for an equivalent circuit presented in Figure 18. The fitted parameters are given in Figures 19-21.



**Figure 18.** Equivalent circuit for SbSI@CNT gel prepared ultrasonically in methanol [13].

Every semiconducting ferroelectric SbSI nanowire (in CNT) can be represented by parallel connection of resistance and capacitance. There appear a few groups of possible explanation of physical origin of CPEs:

1. CPE can be related to macroscopic heterogeneities (porosity, grain sizes, surface roughness, etc.) occurring at the sample electrodes [67];
2. CPE can be associated with ion (anion) adsorption at the roughened electrodes [67];
3. CPE can be related to random mixtures of a conductor and an insulator that can be described by the effective medium approximation [68];
4. CPE can be due to distribution of activation energy of the reduction process [69];
5. CPE can also include contributions from dynamic disorders such as diffusion [68].

In the present case, we are able to offer (after [70]) some additional suggestions, as follows. The CPE represents time-dependent phenomena which, in the case of polarization fluctua-

tions, may be an indicator of the cooperative nature of the fluctuations of individual dipoles. Specifically, fluctuating dipoles interact with their surroundings.

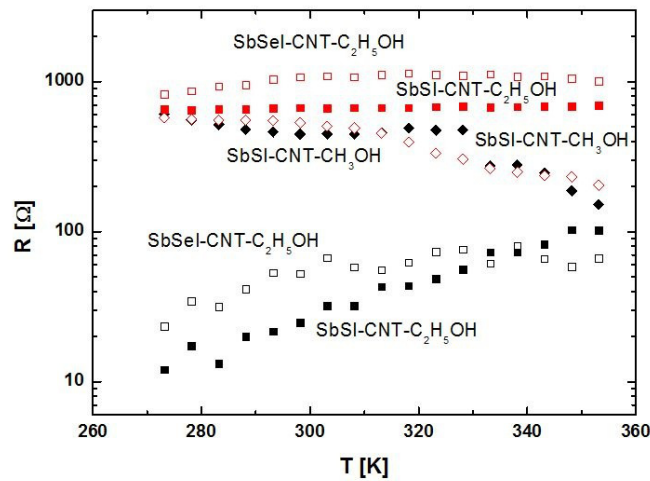


**Figure 19.** Comparison of the temperature dependences of resistance parameters of the equivalent circuits describing Nyquist plots registered in the cases of SbSI@CNT ultrasonically prepared in methanol [ $\diamond - R_1, \blacklozenge - R_2$ ] (Figures 17 and 18), and SbSI@CNT ( $\blacksquare - R_1, \blacksquare - R_2$ ) and SbSel@CNT ( $\square - R_1, \square - R_2$ ) ultrasonically prepared in ethanol.

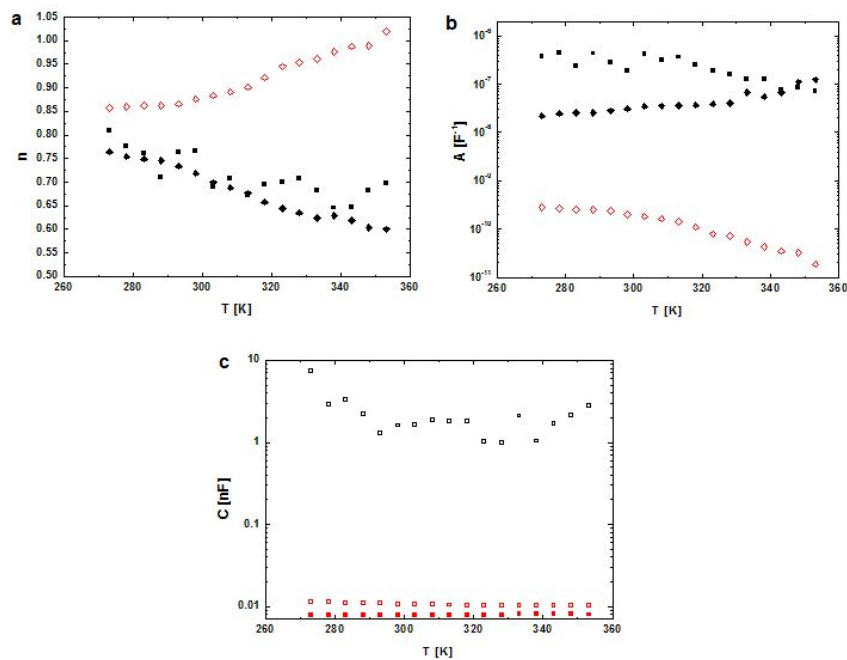


**Figure 20.** Comparison of the temperature dependences of capacitance parameters of the equivalent circuits describing Nyquist plots registered in the cases of SbSI@CNT ultrasonically prepared in methanol [ $\blacklozenge - n_1, A_1; \diamond - n_2, A_2$ ] (Figures 17 and 18), and SbSI@CNT ( $\blacksquare - n, A; \blacksquare - C$ ) and SbSel@CNT ( $\blacksquare - C_1, \square - C_2$ ) ultrasonically prepared in ethanol.

In order to interpret experimental data, it is essential to have a model equivalent circuit that provides a realistic representation of the sample. The investigated SbSI@CNT and SbSeI@CNT gel is a complicated object that contains carbon nanotubes (filled with SbSI or SbSeI) connected with each other in parallel and in series, as well as interfaces (i.e. nanowires - nanowires or nanowires - electrodes). Of course the models should not possess too many components, because the fitting of many variables will be unreliable. Therefore the interpretation of the components of the equivalent electric circuits presented in Figure 18 is very difficult. To obtain simpler image of the observed phenomena experiments with single SbSI@CNT and SbSeI@CNT are needed.

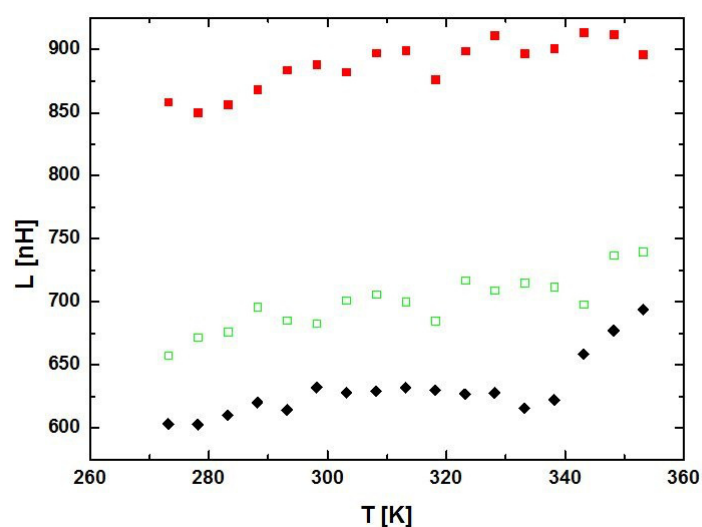


**Figure 21.** Comparison of the temperature dependences of inductance parameters of the equivalent circuits describing Nyquist plots registered in the cases of SbSI@CNT ultrasonically prepared in methanol [13] ( $\blacklozenge$ ) (Figures 17 and 18), and SbSI@CNT ( $\blacksquare$ ) and SbSeI@CNT ( $\square$ ) ultrasonically prepared in ethanol.

Figure 22 presents comparison of the temperature dependences of relaxation time of SbSI@CNT ultrasonically prepared in methanol with the relaxation time of SbSI@CNT and SbSeI@CNT ultrasonically prepared in ethanol. One can see the influence of the liquid used during sonochemical filling of CNTs on properties of the product. In the case of SbSI@CNT ultrasonically prepared in methanol there are two relaxation times in temperatures lower than  $T=293$  K. Above this temperature only one relaxation time is needed to describe the properties of SbSI@CNT. Such behavior can be connected with the ferroelectric-paraelectric phase transition of SbSI near Curie temperature  $T_c=292(1)$  K [17,18]. This phenomenon needs additional investigations.

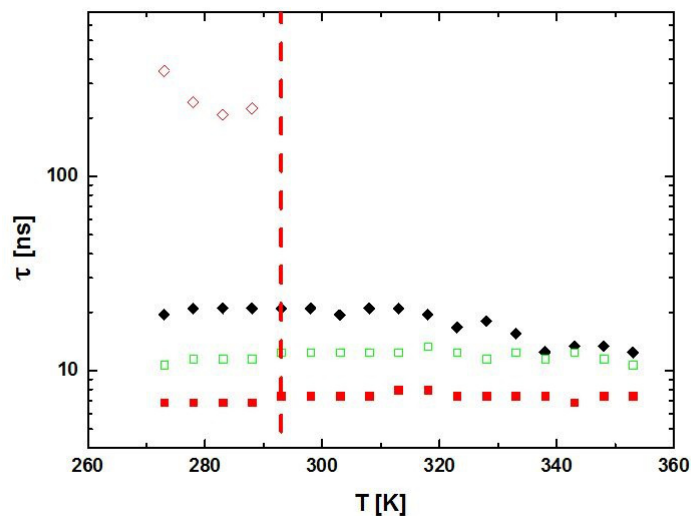


**Figure 22.** Comparison of the temperature dependences of relaxation time of SbSI@CNT ultrasonically prepared in methanol ( $\blacklozenge - \tau_1$ ,  $\redlozenge - \tau_2$ ) (Figure 17), and SbSI@CNT ( $\redsquare$ ) and SbSeI@CNT ( $\green square$ ) ultrasonically prepared in ethanol [13].

It should be noted, that similar equivalent circuits have been well fitted to the Nyquist plots registered also in the cases of SbSI@CNT and SbSeI@CNT ultrasonically prepared in ethanol. Comparison of the temperature dependences of the fitted parameters are given in Figures 19-21.

To overcome the mentioned above problems with interfaces (i.e., nanotubes - nanotubes and nanotubes - electrodes), an essential prerequisite is to build reliable interconnections between the CNTs and the external electrical circuits. To address this need, various chemical and physical processes have been explored to build such interconnections [71]. Changxin Chen et al. [72,73] have presented ultrasonic nanowelding process, with which one can fabricate reliable bonding between SWCNTs and metal electrodes. Ultrasonic nanowelding was carried out in a FB-128 ultrasonic wire bonder [72,73]. An  $\text{Al}_2\text{O}_3$  single crystal with a  $2,500 \mu\text{m}^2$  circular pressing surface and a RMS roughness of 0.2 nm was mounted onto the bonder to act as the welding head. A clamping force of 78.4 mN was applied to press the welding head against the nanotube and electrodes. At the same time an ultrasonic vibration with a frequency of 60 kHz and an ultrasonic power of about 10 mW was applied to the welding head through an ultrasonic transducer. The ultrasonic energy was transferred to the bonding interface through the ultrasonic welding head. Thus the ends of SWCNTs and electrodes were welded together under the combined action of the ultrasonic energy and a clamping force. The welding process was carried out at room temperature for a duration of 0.2 s.

Figure 23 presents SEM and AFM images of carbon nanotubes on Si/SiO<sub>2</sub> substrate with Au electrodes after ultrasonic welding. In our ultrasonic nanowelding set-up the generator ADG70-100P-230-NO 70 kHz (Rinco Ultrasonics) with converter C 70-2 (Rinco Ultrasonics) has been used. The sonotrodes have been equipped with SiC single crystals. The preliminary

electrical tests of SbSI@CNTs ultrasonic nanowelded with different microelectrodes on different substrates are successful. The obtained results will be published in a near future.

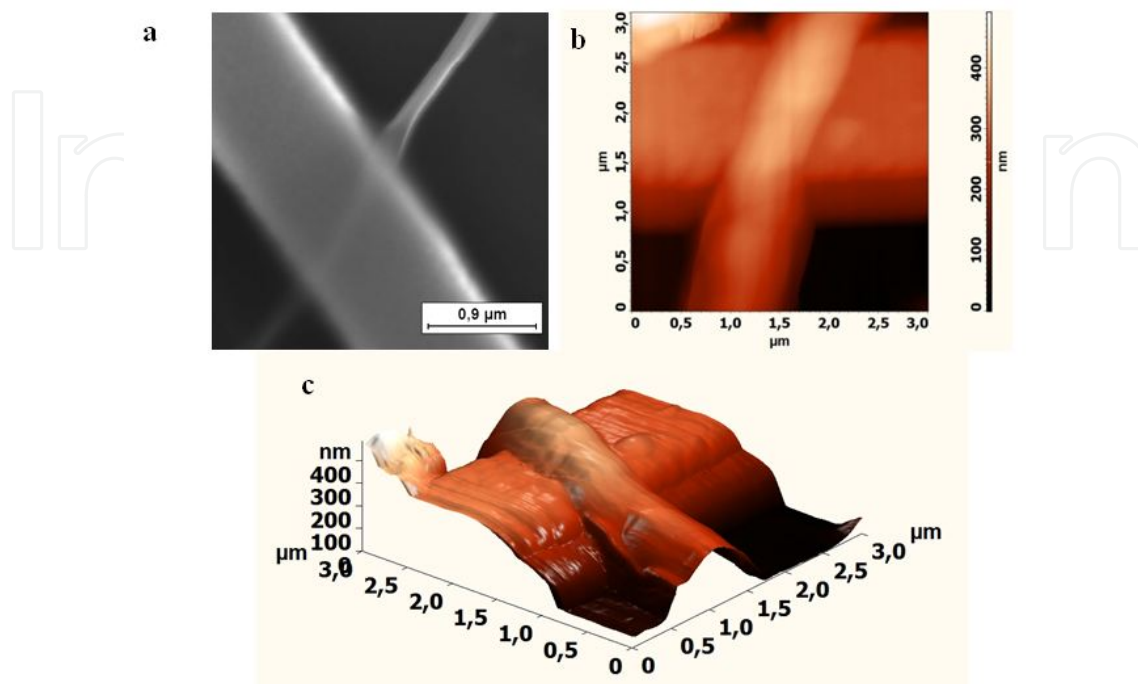


**Figure 23.** SEM and AFM images of carbon nanotubes on Si/SiO<sub>2</sub> substrate with Au electrodes after ultrasonic welding.

## 5. Conclusions

The presented very simple, sonochemical synthesis of nanophase SbSI or SbSeI in CNTs at low temperature is a convenient, fast, mild, efficient and environmentally friendly route for producing novel type of hybrid nanomaterials. The resulting SbSI@CNTs and SbSeI@CNTs composites are highly anisotropic 1D structures whose electronic and optical properties are considerably modified with respect to the encapsulating nanotube. The fabricated SbSI and SbSeI fillings of CNTs are single crystalline in nature and in the form of nanowires.

Since the sonochemical process was carried out at ambient temperature and pressure, it may be predicted that upscaling of this method will lead to large quantities of SbSI@CNTs and SbSeI@CNTs. Further studies on the properties of the sonochemically prepared SbSI and SbSeI in CNTs are underway. Taking into account the recently reported sonochemical preparation of pure SbS<sub>1-x</sub>Se<sub>x</sub>I nanowires [36], one should expect the sonochemical preparation of quaternary SbS<sub>1-x</sub>Se<sub>x</sub>I semiconductors within CNTs. The possibility of change the energy gap (and other parameters) with changing molar composition (x) of the quaternary compounds [36] gives opportunity to tail the functional properties of CNTs filled with SbS<sub>1-x</sub>Se<sub>x</sub>I. It should be remember that the physical properties of such quaternary compounds, formed as solid solutions, can be tailored with stoichiometric composition. It should be an advantage

of using such material in different devices. It seems that this approach can be extended to the preparation of some other ternary and quaternary nanomaterials formed from the group 15-16-17 elements within CNTs. It should provide a "bottom-up" approach for the manufacture of future nanoscale devices.

This review summarizes all so far published results of investigations on SbSI@CNTs and SbSeI@CNTs. One can see that the properties of these 1D hybrid nanomaterials still remain little known. Meantime, these nanostructures should provide promising materials for fundamental investigations on nanoscale ferroelectricity and piezoelectricity as well as materials for some applications.

Obviously, the presented new materials as the other one-dimensional semiconductor nanostructures should receive considerable attention from the scientific and engineering communities due to their potentially useful novel electronic properties.

The ultrasonic nanowelding of SbSI@CNTs and SbSeI@CNTs with metal microelectrodes meets the need of future large-scale, simply, convenient, fast, and efficient technology to build reliable interconnections between the CNTs filled with ternary chalcogenides formed from the group 15–16–17 elements and the external electrical circuits.

## Acknowledgements

The authors are indebted to Dr. P. Szperlich, Prof. J. Szala, Prof. S. Kochowski, Dr. A. Starczewska, Dr. M. Kępińska, and Dr. T. Rzychoń of the Silesian University of Technology, Katowice (Poland), and Prof. D. Stróż and Prof. R. Wrzalik of the University of Silesia, Katowice (Poland) for collaboration in investigations of carbon nanotubes filled with ternary chalcogenides. This review was partially supported by the NCN (Poland) under contract No. UMO-2011/01/B/ST5/06273.

## Author details

Marian Nowak\* and Marcin Jesionek

\*Address all correspondence to: Marian.Nowak@polsl.pl

Institute of Physics, Silesian University of Technology, Poland

## References

- [1] Iijima, S. (1991). Helical microtubules of graphitic carbon. *Nature*, 354, 56-58.
- [2] Ajayan, P. M., & Iijima, S. (1993). Capillarity-induced filling of carbon nanotubes. *Nature*, 361, 333-334.

- [3] Ugarte, D., Stöckli, T., Bonard, J. M., Châtelain, A., & de Heer, W. A. (1998). Filling carbon nanotubes. *Appl. Phys. A*, 67, 101-105.
- [4] Monthieux, M. (2002). Filling single-wall carbon nanotubes. *Carbon*, 40, 1809-1823.
- [5] Tasis, D., Tagmatarchis, N., Bianco, A., & Prato, M. (2006). Chemistry of Carbon Nanotubes. *Chem. Rev.*, 106, 1105-1136.
- [6] Rakov, Eduard G. (2006). Chemistry of Carbon Nanotubes. Chapter 5, in *Nanomaterials Handbook*, Taylor & Francis Group, LLC.
- [7] Eliseev, A., Yashina, L., Kharlamova, M., & Kiselev, N. (2011). One-Dimensional Crystals inside Single-Walled Carbon Nanotubes: Growth, Structure and Electronic Properties. In: J. M. Marulanda (Ed.) *Electronic Properties of Carbon Nanotubes*, Rijeka: In-Tech, 127-156, <http://www.intechopen.com/books/electronic-properties-of-carbon-nanotubes/one-dimensional-crystals-inside-single-walled-carbon-nanotubes-growth-structure-and-electronic-prope>, accessed 21 June 2012).
- [8] Lukanov, P., Tîlmaciu, C. - M., Galibert, A. M., Soula, B., & Flahaut, E. (2011). Filling of Carbon Nanotubes with Compounds in Solution or Melted Phase. in: R. Klingeler, R. B. Sim (eds.) *Carbon Nanotubes for Biomedical Applications*, Carbon Nanostructures, Berlin: Springer-Verlag.
- [9] Sloan, J., Grosvenor, S. J., Friedrichs, S., Kirkland, A. I., Hutchison, J. L., & Green, M. L. H. (2002). A One-Dimensional Ba<sub>2</sub> Chain with Five- and Six-Coordination, Formed within a Single-Walled Carbon Nanotube, *Angew. Chem. Int. Ed*, 41, 1156-1159.
- [10] Fan, X., Dickey, E. C., Eklund, P. C., Williams, K. A., Grigorian, L., Buczko, R., Pantelides, S. T., & Pennycook, S. J. (2000). Atomic Arrangement of Iodine Atoms inside Single-Walled Carbon Nanotubes. *Phys. Rev. Lett*, 84, 4621-4624.
- [11] Nowak, M., Jesionek, M., Szperlich, P., Szala, J., Rzychoń, T., & Stróż, D. (2009). Sonochemical growth of antimony sulfoiodide in multiwalled carbon nanotube, *Ultrason. Sonochem*, 16, 800-804.
- [12] Stróż, D., Nowak, M., Jesionek, M., & Bałdys, K. (2010). Structure of antimony sulfoiodide ultrasonically prepared in carbon nanotubes. *Solid State Phenomena*, 163, 88-92.
- [13] Jesionek, M. (2011). Preparation and properties of hybrid materials containing nanocrystalline SbSI and SbSeI in carbon nanotubes (in Polish). *PhD thesis. Institute of Physics, University of Silesia, Katowice*.
- [14] Jesionek, M., Nowak, M., Szperlich, P., Stróż, D., Szala, J., Jesionek, K., & Rzychoń, T. (2012). Sonochemical growth of antimony selenoiodide in multiwalled carbon nanotube, *Ultrason. Sonochem*, 19, 179-185.
- [15] Nowak, M., Szperlich, P., Bober, Ł., Szala, J., Moskal, G., & Stróż, D. (2008). Sonochemical Preparation of SbSI Gel, *Ultrason. Sonochem*, 15, 709-716.

- [16] Nowak, M., Mroczek, P., Duka, P., Kidawa, A., Szperlich, P., Grabowski, A., Szala, J., & Moskal, G. (2009). Using of textured polycrystalline SbSI in actuators. *Sensors and Actuators A*, 150, 251-256.
- [17] Nowak, M. (2010). Photoferroelectric nanowires. in: N. Lupu (Ed.) *Nanowires Science and Technology*. Rijeka: InTech, 269-308, <http://www.intechopen.com/articles/show/title/photoferroelectric-nanowires>, accessed 21 June 2012).
- [18] Szperlich, P., Nowak, M., Bober, Ł., Szala, J., & Stróż, D. (2009). Ferroelectric properties of ultrasonochemically prepared SbSI ethanogel. *Ultrason. Sonochem*, 16, 398-401.
- [19] Nowak, M., Kauch, B., Szperlich, P., Jesionek, M., Kępińska, M., Bober, Ł., Szala, J., Moskal, G., Rzychoń, T., & Stróż, D. (2009). Sonochemical Preparation of SbSeI Gel. *Ultrason. Sonochem*, 16, 546-551.
- [20] Suslick, K. S., & Price, G. J. (1999). Applications of ultrasound to materials chemistry. *Annu. Rev. Mater. Sci*, 29, 295-326.
- [21] Jin, Ho. Bang, & Suslick, K. S. (2010). Applications of Ultrasound to the Synthesis of Nanostructured Materials. *Adv. Mater*, 22, 1039-1059.
- [22] Abedini, R., & Mousavi, S. M. (2010). Preparation and enhancing of materials using ultrasound technique: polymers, catalysts and nano-structure particles. *Petroleum & Coal*, 52, 81-98.
- [23] Mason, T. J. (2003). Sonochemistry and sonoprocessing: the link, the trends and (probably) the future,. *Ultrason. Sonochem*, 10, 175-179.
- [24] Gedanken, A. (2004). Using sonochemistry for the fabrication of nanomaterials,. *Ultrason. Sonochem*, 11, 47-55.
- [25] Cravotto, G., & Cintas, P. (2006). Power ultrasound in organic synthesis: moving cavitation chemistry from academia to innovative and large-scale applications. *Chem. Soc. Rev*, 35, 180-196.
- [26] Suslick, K. S., Didenko, Y., Fang, M. M., Hyeon, T., Kolbeck, K. J., Mc Namara, W. B., Mdleleni, M. M., & Wong, M. (1999). Acoustic cavitation and its chemical consequences. *Phil. Trans. Roy. Soc. A*, 357, 335-353.
- [27] Ibanez, A., Jumas, J. C., Olivier-Fourcade, J., Philippot, E., & Maurin, M. (1983). On chalcogenide-iodates of antimony SbXI (X=S, Se, Te): structure and Mossbauer spectra of  $^{121}\text{Sb}$ . *J. Solid State Chem*, 48, 272-283.
- [28] Antimony Selenide Iodide (2000). JCPDS-International Centre for Diffraction Data. PCPDFWIN Card File , 2(76-1354)
- [29] Hassel, O., & Mark, H. (1924). Über die Kristallstruktur des Graphits. *Z. Phys*, 25, 317-337.
- [30] Carbon (2000). JCPDS-International Centre for Diffraction Data. PCPDFWIN Card File , 2(75-1621)

- [31] Pohl, S., & Saak, W. (1984). Zur Polymorphie von Antimontriiodid. Die Kristallstruktur von monoklinem  $\text{SbI}_3$ . *Z. Kristallogr*, 169, 177-184.
- [32] Antimony Iodide (2000). JCPDS-International Centre for Diffraction Data. PCPDFWIN Card File , 2(75-1417)
- [33] Antimony Sulfide Iodide (2000). JCPDS-International Centre for Diffraction Data. PCPDFWIN Card File , 2(74-0149)
- [34] Starczewska, A., Wrzalik, R., Nowak, M., Szperlich, P., Jesionek, M., Moskal, G., Rzychoń, T., Szala, J., Stróż, D., & Maślanka, P. (2009). Influence of the solvent on ultrasonically produced SbSI nanowires. *Ultrason. Sonochem*, 16, 537-545.
- [35] Properties of inorganic compounds. (2012). National Physics Laboratory. [http://www.kayelaby.npl.co.uk/chemistry/3\\_2/3\\_2.html](http://www.kayelaby.npl.co.uk/chemistry/3_2/3_2.html), accessed 21 June).
- [36] Nowak, M., Kauch, B., Szperlich, P., Stróż, D., Szala, J., Rzychoń, T., Bober, Ł., Toroń, B., & Nowrot, A. (2010). Sonochemical preparation of  $\text{SbS}_{1-x}\text{Se}_x\text{I}$  nanowires. *Ultrason. Sonochem*, 17, 487-493.
- [37] Nowak, M., Talik, E., Szperlich, P., & Stróż, D. (2009). XPS analysis of sonochemically prepared SbSI ethanogel. *Appl. Surf. Sci*, 255, 7689-7694.
- [38] Nowak, M., Szperlich, P., Talik, E., Szala, J., Rzychoń, T., Stróż, D., Nowrot, A., & Sol-ecka, B. (2010). *Ultrason. Sonochem*, 17, 219-227.
- [39] Sloan, J., Cook, J., Chu, A., Zwiefka-Sibley, M., Green, M. L. H., & Hutchison, J. L. (1998). Selective Deposition of  $\text{UCl}_4$  and  $(\text{KCl})_x(\text{UCl}_4)_y$  inside Carbon Nanotubes Using Eutectic and Noneutectic Mixtures of  $\text{UCl}_4$  with KCl. *J. Solid State Chem*, 140, 83-90.
- [40] Rolsten, R. F. (1961). Iodide Metals and Metal Iodides. *New York: Wiley*.
- [41] Mizukoshi, Y., Nakamura, H., Bandow, H., Maeda, Y., & Nagata, Y. (1999). Sonolysis of organic liquid: effect of vapour pressure and evaporation rate. *Ultrason. Sonochem*, 6, 203-209.
- [42] Gutiérrez, M., & Henglein, A. (1988). Sonolytic decomposition of poly(vinylpyrrolidone), ethanol, and tetranitromethane in aqueous solution. *J. Phys. Chem*, 92, 2978-2981.
- [43] Li, B., Xie, Y., Huang, J., & Qian, Y. (1999). Sonochemical synthesis of silver, copper and lead selenides. *Ultrason. Sonochem*, 6, 217-220.
- [44] Li, H.- L., Zhu, Y.- C., Chen, S.- G., Palchik, O., Xiong, J.-P., Kolytyn, Yu., Gofer, Y., & Gedanken, A. (2003). A novel ultrasound-assisted approach to the synthesis of CdSe and CdS nanoparticles. *J. Sol. State Chem*, 172, 102-110.
- [45] Lu, K. L., Lago, R. M., Chen, Y. K., Green, M. L. H., Harris, P. J. F., & Tsang, S. C. (1996). Mechanical Damage of Carbon Nanotubes by Ultrasound. *Carbon*, 34, 814-816.

- [46] Chunwei, Yang., Xinguo, Hu., Dianlong, Wang., Changsong, Dai., Liang, Zhang., Haibo, Jin., & Simeon, Agathopoulos. (2006). Ultrasonically treated multi-walled carbon nanotubes (MWCNTs) as PtRu catalyst supports for methanol electrooxidation. *J. Power Sources*, 160, 187-193.
- [47] Eletsii, A. V. (2004). Sorption properties of carbon nanostructures. *Physics-Uspokhi*, 47, 1119-1154.
- [48] Qiang, F. U., Weinberg, G., & Dang-sheng, S. U. (2008). Selective filling of carbon nanotubes with metals by selective washing. *New Carbon Materials*, 23, 17-20.
- [49] De Gennes, P. G., Brochard-Wyart, F., & Quere, D. (2003). Capillarity and Wetting Phenomena: Drops, Bubbles, Pearls, Waves. *Berlin: Springer*, 51-52.
- [50] Voutsas, G. P., & Rentzeperis, P. J. (1986). The crystal structure of the quaternary compound  $\text{SbSe}_{0.75}\text{S}_{0.25}$ . *Z. Kristallogr*, 178, 289-295.
- [51] Molnar, B., Johannes, R., & Haas, W. (1965). Properties of single-crystal SbSI. *Bull. Am. Phys. Soc*, 10, 109.
- [52] Gerzanich, E. I., Lyakhovitskaya, V. A., Fridkin, V. M., & Popovkin, B. A. (1982). in: *E. Kaldis (Ed.), Current Topics in Materials Science, Amsterdam: North-Holland*, 10, 55-190.
- [53] Pankove, J. I. (1971). Optical processes in semiconductors. *New Jersey: Prentice-Hall Inc.*
- [54] Kortum, G. (1969). Reflectance Spectroscopy. *Berlin: Springer-Verlag*.
- [55] Philips-Invernizzi, B., Dupont, D., & Caze, C. (2001). Bibliographical review for reflectance of diffusing media. *Opt. Eng*, 40, 1082-1092.
- [56] Dahm, D. J., & Dahm, K. D. (2007). Interpreting Diffuse Reflectance and Transmittance: A Theoretical Introduction to Absorption Spectroscopy of Scattering Materials. *Norfolk: IM Publications LLP*.
- [57] Nowak, M., Kauch, B., & Szperlich, P. (2009). Determination of energy band gap of nanocrystalline SbSI using diffuse reflectance spectroscopy. *Rev. Sci. Instrum*, 80, 046107.
- [58] Dong-Woon, Shin., Seung-Cheol, Hyun., Sang-An, Park., Yoeng-Geun, Kim., Chang-Dae, Kim., & Wha-Tek, Kim. (1994). Optical properties of undoped and Ni-doped V-VI-VII single crystals. *J. Phys. Chem. Solids*, 55, 825-830.
- [59] Seung-Cheol, Hyun., Young-Geun, Kim., Mi-Yang, Kim., Jeong-Dae, Koh., Byong-Seo, Park., & Wha-Tek, Kim. (1995). Optical properties of undoped and chromium-doped  $\text{V}^{\text{A}}\text{-VI}^{\text{A}}\text{-VII}^{\text{A}}$  single crystals. *J. Mater. Sci*, 30, 6113-6117.
- [60] Sang-An, Park., Mi-Yang, Kim., Ji-Young, Lim., Byong-Seo, Park., Jeong-Dae, Koh., & Wha-Tek, Kim. (1995). Optical Properties of Undoped and V-Doped  $\text{VA-VIA-VIIA}$  Single Crystals. *Phys. Status Solidi B*, 187, 253-260.

- [61] Soonie, Jeon., Gijun, Cho., Wha-tek, Kim., & Sook-II, Kwun. (1988). *Solid State Commun*, 68, 1043-1046.
- [62] Yeong-Koo, Baik., Jae-Keun, Kim., Wha-Tek, Kim., & Sook-II, Kwun. (1988). Optical Properties of SbSI:Co and SbSeI : Co Single Crystals. *New Phys. (Korean Physical Society)*, 28, 291-295.
- [63] Barsoukov, E., & Macdonald, J. R. (2005). *Impedance Spectroscopy Theory, Experiment, and Applications. 2nd edition, Wiley, New Jersey.*
- [64] ZView Version 3.1c, Copyright. (2007). Scribner Associates. *Inc. written by Derek Johnson.*
- [65] Tselev, A., Woodson, M. , Ch, Qian. , & Liu, J. (2008). Microwave Impedance Spectroscopy of Dense Carbon Nanotube Bundles. *Nano Lett.*, 8, 152-156.
- [66] Plombon, J. J., O'Brien, K. P., Gstrein, F., & Dubin, V. M. (2007). High-frequency electrical properties of individual and bundled carbon nanotubes. *Applied Physics Lett*, 90, 063106.
- [67] Barsoukov, E., & Macdonald, J. R. (2005). *Impedance Spectroscopy, Theory, Experiment and Applications. 2nd edition, Wiley-Interscience, New York.*
- [68] Metikos-Hukovic, M., Omanovic, S., & Jukic, A. (1999). Impedance spectroscopy of semiconducting films on tin electrodes. *Electrochimica Acta*, 45, 977-986.
- [69] Ricciardi, S., Ruiz-Morales, J. C., & Nuñez, P. (2009). Origin and quantitative analysis of the constant phase element of a platinum SOFC cathode using the state-space model. *Solid State Ionics*, 180, 1083-1090.
- [70] Osman, R. A. M., & West, A. R. (2011). Electrical characterization and equivalent circuit analysis of  $(\text{Bi}_{1.5}\text{Zn}_{0.5})(\text{Nb}_{0.5}\text{Ti}_{1.5})\text{O}_7$  Pyrochlore, a relaxor ceramic. *Journal of Applied Physics*, 109, 074106-8.
- [71] Changxin, Chen., & Yafei, Zhang. (2009). Nanowelded Carbon Nanotubes. From Field-Effect Transistors to Solar Microcells,. *Series: NanoScience and Technology, Springer, Chapter 4: Ultrasonic Nanowelding Technology Between Carbon Nanotubes and Metal Electrodes*, 978-3-642-01498-7, 47-62.
- [72] Changxin, Chen., Liyue, Liu., Yang, Lu., Eric-Wai, Siu., Kong, Yafei., Zhang, Xinjun., & Sheng, Han. Ding. (2007). A method for creating reliable and low-resistance contacts between carbon nanotubes and microelectrodes. *Carbon*, 45, 436-442.
- [73] Changxin, Chen., Liyue, Liu., Yang, Lu., Eric-Wai, Siu., Kong, Yafei., Zhang, Xinjun., Sheng, Han., & Ding, . (2007). Corrigendum to "A method for creating reliable and low-resistance contacts between carbon nanotubes and microelectrodes". *Carbon*, 45, e1, 436-442.

IntechOpen

IntechOpen